

**A climatology of nonmigrating semidiurnal  
tides from TIMED Doppler Interferometer  
(TIDI) wind data**

J. Oberheide<sup>a,\*</sup>, Q. Wu<sup>b</sup>, T. L. Killeen<sup>b</sup>, M. E. Hagan<sup>b</sup>, and  
R. G. Roble<sup>b</sup>

<sup>a</sup>*Physics Department, University of Wuppertal, 42097 Wuppertal, Germany*

<sup>b</sup>*High Altitude Observatory, National Center for Atmospheric Research, Boulder,  
CO, USA*

---

1 **Abstract**

2 With the launch of the TIMED satellite in December 2001, continuous tempera-  
3 ture and wind data sets amenable to MLT tidal analyses became available. The  
4 wind measuring instrument, the TIMED Doppler interferometer (TIDI), is operat-  
5 ing since early 2002. Its day- and nighttime capability allows to derive tidal winds  
6 over a range of MLT altitudes. This paper presents climatologies (June 2002 to  
7 June 2005) of monthly mean amplitudes and phases for 6 nonmigrating semidiur-  
8 nal tidal components between 85 and 105 km altitude and between 45°S and 45°N  
9 latitude (westward propagating wave numbers 4, 3, 1; the standing oscillation s0;  
10 and eastward propagating wave numbers 1, 2) in the zonal and meridional wind  
11 directions.

12 Amplitude errors are 15-20 % (accuracy) and 0.8 m/s (precision). The phase error  
13 is 2 hours. The TIDI analysis agrees well with 1991-1994 UARS results at 95 km.  
14 During boreal winter, amplitudes of a single component can reach 10 m/s at lati-  
15 tudes equatorward of 45°. Aggregate effects of nonmigrating tides can easily reach or  
16 exceed the amplitude of the migrating tide. Comparisons with the global scale wave  
17 model (GSWM) and the thermosphere-ionosphere-mesosphere-electrodynamics gen-  
18 eral circulation model (TIME-GCM) are partly inconclusive but they indicate that  
19 wave-wave interaction and latent heat release in the tropical troposphere play both  
20 an important role in forcing the semidiurnal westward 1, westward 3, and standing  
21 components. Latent heat release is the leading source of the eastward propagating  
22 components.

23 *Key words:* MLT winds, nonmigrating semidiurnal tides, TIDI, TIMED, GSWM,  
24 TIME-GCM

---

## 25 1 Introduction

26 Atmospheric tides are global waves in temperature, winds, and density with  
27 periods that are harmonics of a solar day. They propagate up and away from  
28 their mostly tropospheric and stratospheric sources and transport energy and  
29 momentum from the lower into the middle and upper atmosphere. Hence,  
30 they are essential for understanding vertical coupling processes and for the  
31 dynamics, chemistry, and energetics of Earth's atmosphere. Tidal winds are  
32 on the order of the time-averaged zonal wind and dominate the meridional  
33 wind field in the mesosphere and lower thermosphere (MLT) region. Tidal  
34 temperature oscillations may change reaction rates of chemically active species  
35 with simultaneous transport of air parcels some 1000 km in the horizontal and  
36 some kilometers in the vertical direction (Ward, 1999).

37 Tidal waves are grouped into two classes: (i) the Sun-synchronous (migrat-  
38 ing) tides and (ii) the non-Sun-synchronous (nonmigrating) tides. Migrating  
39 tides propagate westward with the apparent motion of the Sun with a zonal  
40 wave number that equals their frequency in cycles per day. They are primarily  
41 driven by the absorption of solar infrared and ultraviolet radiation in tropo-  
42 spheric water and water vapor, and stratospheric ozone. Non-Sun-synchronous  
43 (nonmigrating) tides are the tidal components that do not follow the appar-  
44 ent westward propagation of the Sun, that is, they may propagate westward,  
45 eastward, or remain standing with zonal wave numbers that do not equal their  
46 frequencies (in cycles per day). Their leading sources are latent heat release  
47 in the tropical troposphere (Hagan and Forbes, 2003, 2002) and the nonlin-

---

\* Corresponding author. Tel.: +49-202-439-2750

*Email address:* [jobberh@uni-wuppertal.de](mailto:jobberh@uni-wuppertal.de) (J. Oberheide).

*URL:* <http://www.atmos.physik.uni-wuppertal.de> (J. Oberheide).

ear interaction between planetary waves and the migrating tide (Lieberman et al., 2004; Forbes et al., 2003; Oberheide et al., 2002; Hagan and Roble, 2001). Hence, nonmigrating tides manifest the influence of large-scale weather systems that cannot propagate through the tropopause into the middle and upper atmosphere. Recent ionospheric ultraviolet emission measurements by FUV-IMAGE and GUVI/TIMED indicate that the effects of nonmigrating tides extend well into the F-layer via a longitude modulation of the E-layer dynamo electric fields (Immel et al., 2006).

Triggered by the growing appreciation of their importance, nonmigrating tides have been the target of increasing research activities by both experimenters and modelers during the past few years. In this work, only nonmigrating tides of semidiurnal period are considered. For an overview of recent diurnal analyses, see Oberheide et al. (2006) and references therein.

Tidal and general circulation models have been used to study semidiurnal nonmigrating tidal sources and morphology (Ward et al., 2005; Mayr et al., 2005; Hagan and Forbes, 2003; Grieger et al., 2002; Yamashita et al., 2002). These simulations gave an idea of the latent heat and planetary wave - tidal interaction forcing mechanisms and the spatio-temporal amplitude and phase distributions. A quantitative assessment of the model predictions and the underlying parameterizations, however, is an open issue which is primarily due to the lack of observation-based tidal definitions. The few observational results rather indicate that the present model understanding is in fact more qualitative with frequent discrepancies in both tidal magnitudes and spatio-temporal distributions.

Nonmigrating semidiurnal tides have been analyzed from ground-based mea-

73 surements in Antarctica (Baumgaertner et al., 2006; Lau et al., 2006; Hibbins  
74 et al., 2006; Murphy et al., 2003) thereby extending the earlier results of Forbes  
75 et al. (1999), at northern high latitudes (Wu et al., 2003) and at northern mid-  
76 latitudes (Pancheva et al., 2002). Climatological information about the global  
77 structure comes predominantly from satellite analyses. Amplitudes and phases  
78 have been recently derived from SABER and MLS temperature measurements  
79 (Forbes and Wu, 2006; Forbes et al., 2006; Zhang et al., 2006). Unfortunately,  
80 the analysis of nonmigrating semidiurnal tides in MLT winds has so far been  
81 limited to 95 km altitude based upon measurements from HRDI and WINDII  
82 on board UARS (Huang and Reber, 2004; Manson et al., 2004; Cierpik et al.,  
83 2003; Angelats i Coll and Forbes, 2002).

84 However, with the launch of the TIMED satellite in December 2001, continu-  
85 ous wind data from the TIMED Doppler Interferometer (TIDI) (Killeen et al.,  
86 2006) amenable to nonmigrating tidal analyses over a range of MLT altitudes  
87 became available. They have already been analyzed on nonmigrating diurnal  
88 tides in an earlier paper (Oberheide et al., 2006). The present work extends  
89 this analysis to the semidiurnal tides. Climatologies (June 2002 to June 2005)  
90 of monthly mean amplitudes and phases are derived for 6 semidiurnal tidal  
91 components between 85 and 105 km altitude and between 45°S and 45°N lat-  
92 itude (westward propagating wave numbers 4, 3, 1; the standing oscillation  
93 s0; and eastward propagating wave numbers 1, 2) in the zonal and meridional  
94 wind directions. The TIDI climatologies are compared to HRDI and WINDII  
95 analyses from Angelats i Coll and Forbes (2002) at 95 km and to model sim-  
96 ulations of the global scale wave model (GSWM, Hagan and Forbes (2003))  
97 and the thermosphere-ionosphere-mesosphere-electrodynamics general circu-  
98 lation model (TIME-GCM, Roble and Ridley (1994)). This allows to assess

99 the model prediction capabilities and to study the tidal forcing mechanisms.

100 The paper is organized as follows. The TIDI data and the tidal analysis method  
101 are described in section 2, including error estimates. Tidal climatologies are  
102 presented in section 3 and compared to HRDI and WINDII analysis in section  
103 4. Model comparisons and tidal forcing mechanisms are discussed in section  
104 5. Concluding remarks are given in section 6.

## 105 **2 Data and Analysis**

### 106 *2.1 TIDI Measurements*

107 The instrument on board the TIMED satellite with the primary objective  
108 to measure winds in the MLT region is the TIMED Doppler Interferometer  
109 (TIDI). It was developed and built by the University of Michigan. See Killeen  
110 et al. (2006) for an overview and recent results. Daytime and nighttime neutral  
111 winds are measured by limb scanning various upper atmosphere airglow layers  
112 and monitoring the Doppler shift. TIDI has four telescopes that are orthog-  
113 onally orientated ( $45^\circ$  with respect to the orbit). This allows the instrument  
114 to measure wind vectors on both sides of the satellite track (i.e., cold and  
115 warm sides). The viewing directions of the two telescopes on the same side of  
116 the spacecraft are perpendicular to one another such that the same locations  
117 are observed with a time delay of a few minutes when the satellite moves  
118 forward. The samplings in the two directions are then used to form the neu-  
119 tral wind vector in terms of the zonal (eastward) and meridional (northward)  
120 components.

121 Data are taken from pole-to-pole with a vertical resolution of 2.5 km and an  
122 along track resolution of about 800 km. The present nonmigrating tidal anal-  
123 ysis covers the time period from June 2002 to June 2005. TIDI data used here  
124 are O<sub>2</sub> (0-0) band P9 vector winds (level3, data versions 00\_01 (2002), 01\_01 to  
125 01\_03 (2003), 03\_03 (2004), 03\_04 (2005)) between 85 and 105 km altitude that  
126 were produced by the National Center for Atmospheric Research (NCAR).  
127 They may be downloaded from <http://timed.hao.ucar.edu/tidi/>. TIDI has  
128 continuously taken data with one larger data gap in early 2003. The instru-  
129 ment operational performance has been nominal except for two anomalies that  
130 are now well understood: (1) higher than expected background white light and  
131 (2) ice deposition on cold surfaces. Instrumental modes and data analysis tech-  
132 niques have been adjusted to mitigate their effects on data quality (Killeen  
133 et al., 2006). These efforts reduced the noise level of individual wind profiles  
134 that were previously assumed to be 30 m/s during the day and double that  
135 during the night (Oberheide et al., 2006).

136 Measuring simultaneously on both sides of the satellite track provides four  
137 local solar time (LST) samplings equatorward of  $\pm 60^\circ$  and two at latitudes  
138 poleward of  $\pm 60^\circ$ . For a given latitude, the LSTs of measurements taken on  
139 the ascending (asc) and descending (dsc) orbit nodes can be considered to  
140 be longitude independent for warm and cold side data respectively. The daily  
141 LST variation for a given latitude, side, and orbit node is 12 minutes toward  
142 earlier LST as time progresses. Complete (24 hours) LST coverage is obtained  
143 every 60 days which corresponds to one satellite yaw cycle. The specifics of  
144 TIDI, particularly its day- and nighttime capability, make its wind data set  
145 unprecedented in that it is amenable to global nonmigrating tidal analysis  
146 over a range of MLT altitudes.

148 In the following, all semidiurnal tidal components (propagation direction/wave  
149 number pairs) are identified by using a letter/number combination indicating  
150 both propagation direction (*w*: westward; *s*: standing; *e*: eastward) and zonal  
151 wave number  $s \geq 0$ . For instance, *w1* is the westward propagating nonmi-  
152 grating semidiurnal component of zonal wave number 1, *s0* is the zonally  
153 symmetric (standing) oscillation, and *e2* is the eastward propagating compo-  
154 nent of zonal wave number 2. With the same nomenclature, the migrating  
155 semidiurnal tide is *w2*.

156 The nonmigrating semidiurnal tides are derived exactly as described by Ober-  
157 heide et al. (2006) for their diurnal counterparts. It is basically a two-dimensional  
158 Fourier transform of a 60-day composite data set that is performed in a run-  
159 ning mean sense. Amplitudes and phases are assigned to the day in the middle  
160 of each 60-day period. Hence, nonmigrating tidal amplitudes and phases pre-  
161 sented here must be interpreted in a climatological sense. Short-term tidal  
162 variability cannot be resolved. The present analysis covers the time period  
163 June 2002 to June 2005. Derived amplitudes and phases are averaged into  
164 monthly bins to calculate the tidal climatologies. The details of the analysis  
165 are not repeated here, but two important specifics need to be outlined: (1)  
166 potential zero wind line inconsistencies in the TIDI warm and cold side data  
167 prevent an analysis of the migrating (*w2*) tide because the latter is observed as  
168 a zonally symmetric feature in the satellite data (Oberheide et al., 2003) that  
169 needs to be removed; (2) the inherent smoothing in the set-up of the composite  
170 data requires a scaling of the tidal amplitudes (phases are not affected).

171 The uncertainty in the scaling factors introduces a considerable systematic am-  
172 plitude error (accuracy). Amplitude and phase precisions, on the other hand,  
173 are governed by the measurement noise and the asynoptic satellite sampling.  
174 The scaling factors and errors are calculated in the same way as described  
175 in detail by Oberheide et al. (2006) for the diurnal tides using both model  
176 simulations and the measured data. Amplitude accuracy for the semidiurnal  
177 tides is 15-20%, amplitude precision is about 0.8 m/s, and phase precision is  
178 2 hours (Table 1). The given values are almost independent of latitude and  
179 altitude and apply to the tidal climatologies. Hence, they do not reflect tidal  
180 variability from one year to another. The use of 60-day composite data sig-  
181 nificantly reduces the noise level of the tidal amplitudes and phases, in spite  
182 of the large TIDI noise error of an individual wind measurement. Figure 1  
183 shows an example for the scaled meridional wind amplitudes at 95 km alti-  
184 tude for 15 February 2004 as a function of latitude and zonal wave number.  
185 The amplitude of a single component ( $w_3$ ) exceeds 12 m/s. Note the difference  
186 to Figure 1b in Oberheide et al. (2006) where the unscaled amplitudes were  
187 shown. Semidiurnal tidal analysis is limited to the nonmigrating components  
188  $w_4$ ,  $w_3$ ,  $w_1$ ,  $s_0$ ,  $e_1$ , and  $e_2$ . Higher wave numbers require very large scaling  
189 factors with increasing uncertainties such that they are excluded.

### 190 **3 Monthly climatologies**

191 Figures 2 and 3 show two examples for the derived climatologies: the  $w_4$  zonal  
192 wind component (Figure 2) and the  $w_3$  meridional wind component (Fig-  
193 ure 3). Amplitudes are given in m/s and phases are given in universal time  
194 (hours) of maximum amplitude at  $0^\circ$  longitude. For space reasons, it is im-

195 possible to include Figures for all 12 components. Instead, Figures 4 and 5  
196 provide amplitude time-series for all components. The shown altitudes differ  
197 from one component to another. They reflect the altitudes where the basic  
198 features of the respective components are most pronounced. Numerical ampli-  
199 tude and phase values are available on the web ([http://www.atmos.physik.uni-](http://www.atmos.physik.uni-wuppertal.de/causes/nmt_mlt/)  
200 [wuppertal.de/causes/nmt\\_mlt/](http://www.atmos.physik.uni-wuppertal.de/causes/nmt_mlt/)).

201 The w4 zonal wind component (Figure 2) maximizes in boreal winter around  
202 30-40° North and South. The observed maximum amplitude is on the order of  
203 10 m/s with the peak altitude in most cases well above the upper boundary  
204 of the analyzed height interval. Vertical wavelengths during boreal winter are  
205 on the order of 40 km and the phases decrease with increasing height. This is  
206 consistent with upward wave propagation and thus tidal forcing lower in the  
207 atmosphere. Between October and March, the phases are symmetric about the  
208 equator, that is, the tidal wind directions in the Northern and Southern Hemi-  
209 spheres are the same. During the remainder of the year, the phases are more  
210 variable but because the corresponding amplitudes are rather small (except  
211 for latitudes poleward of 40°S), it is difficult to decide whether this variability  
212 is real or not.

213 The w3 meridional wind component (Figure 3) has maximum amplitudes of 8-  
214 10 m/s at 105 km. As for the w4 zonal component, the peak altitude is usually  
215 above the upper boundary of the analyzed height interval. Largest amplitudes  
216 are observed one month before spring and fall equinoxes in March and Septem-  
217 ber with maxima at 40° South and North. Boreal winter amplitudes are still  
218 large with smaller values in boreal summer (2-5 m/s). An equatorial maximum  
219 persists during the whole year. This three peak structure as function of lati-  
220 tude is reflected in the phases that show rapid transitions around 20° North

221 and South where the corresponding amplitudes minimize. The equatorial wind  
222 direction is opposite to that at  $40^\circ$  such that tidal up- or downwelling around  
223  $20^\circ$  latitude is likely, due to mass conservation. Again, the phase decrease  
224 with height indicates a tidal forcing lower in the atmosphere. Estimating the  
225 vertical wavelength is difficult but it is usually on the order of 40 km or above.

226 The further discussion of the TIDI climatologies is now restrained on latitude-  
227 time amplitude distributions. Figure 4 shows the results for the meridional  
228 wind components and their annual mean amplitudes. The w4 component max-  
229 imizes around boreal winter around  $40^\circ$  North and South with peak values of  
230  $\geq 10$  m/s. A smaller, secondary maximum in boreal summer is common for  
231 all observed westward, standing, and eastward components. For the specifics  
232 of w3, see above. The w1 component is highly structured with 4 peaks at or  
233 slightly poleward of  $45^\circ$  and at roughly  $20^\circ$ . The latter are most pronounced  
234 between 90 and 100 km altitude and three phases jumps are observed at the  
235 equator and  $30^\circ$  North and South (not shown). Largest amplitudes occur be-  
236 tween September and April at 105 km. The s0 component generally shows two  
237 maxima at or poleward of  $45^\circ$  and an additional equatorial peak. Amplitudes  
238 reach 5-7 m/s in boreal winter with a considerable month-to-month variation  
239 of the peak altitude from 90-95 km to above 105 km. Phase jumps occur at  
240 latitudes of minimum amplitude (not shown). The e1 component is compara-  
241 tively weak with maximum amplitudes in February and July. The latitudinal  
242 distribution changes from three peaks at  $40^\circ$  and equatorial latitudes in Jan-  
243 uary to two peaks at  $20^\circ$ N and  $30^\circ$ S in July to a single and rather symmetric  
244 peak in November. Phase jumps occur at latitudes of minimum amplitudes  
245 and may be shifted by several degrees latitude from one month to another  
246 (not shown). The e2 component peaks in boreal winter and fall equinox with

247 a broad distribution that is symmetric about the equator. This is also reflected  
248 in the phases (not shown). However, the latitudinal distribution changes to a  
249 three peak structure in boreal summer with phase jumps occurring at latitudes  
250 in between.

251 The time evolution of the zonal wind components (Figure 5) reflects that of  
252 the meridional wind. The latitudinal distributions in both directions may dif-  
253 fer from each other as one may already expect from the classical tidal theory  
254 (Chapman and Lindzen, 1970). The two w4 peaks at 30-40° North and South  
255 have already been discussed above. W3 maximizes around 40° and above 105  
256 km, the smaller equatorial maximum as shown in the Figure is only present  
257 below 100 km. Phase jumps occur at latitudes of minimum amplitude. The  
258 w1 component often peaks poleward of 40° and above 105 km. Boreal summer  
259 amplitudes are comparatively small and maximize between 90-95 km. Equa-  
260 torial peaks are only observed above 95 km and during some months. Phase  
261 transitions occur at latitudes of minimum amplitude. S0 does not show the  
262 equatorial maximum that was present in the meridional wind. Amplitudes are  
263 only 1-2 m/s during most months thus preventing a meaningful discussion of  
264 the corresponding phases. This also applies to e1, that in general shows a simi-  
265 lar amplitude distribution as in the meridional wind. Similar to the meridional  
266 wind, the e2 component is comparatively strong with peak values of  $\geq 5$  m/s in  
267 boreal winter and up to 9 m/s in fall equinox at 105 km. The equinox maxima  
268 are more equatorward than those in boreal winter. Amplitude growth starts in  
269 July and therefore somewhat earlier than observed in most other components.  
270 The general phase behavior is anti-symmetric about the equator (not shown).

271 The large variability of the nonmigrating semidiurnal tides in space and time  
272 together with the narrow latitudinal structure (i.e., 3-4 peaks between 45°S

273 and  $45^\circ\text{N}$  for a number of components) makes their further analysis quite dif-  
274 ficult. This particularly applies to the months with small amplitudes when  
275 the tidal structure is of course more sensitive to external disturbances. Never-  
276 theless, both the latitude-height structures and the time evolutions presented  
277 above show in most cases coherent amplitude and phase structures within the  
278 error bars (section 2.2). This and the following comparison with independent  
279 measurements may give additional confidence in the derived tidal fields.

#### 280 **4 Comparison with UARS**

281 Angelats i Coll and Forbes (2002) provide w1 and w3 meridional wind clima-  
282 tologies from HRDI and WINDII data (in the following referred to as UARS  
283 data). Although their analysis was limited to 95 km altitude and did not in-  
284 clude the zonal winds, it is nevertheless an important data set to compare with.  
285 The UARS data represent monthly averages of the December 1991 through  
286 September 1994 period. Hence, the TIDI comparison with UARS does not  
287 meet the hard requirements of validation. The measurements are almost 11  
288 years apart in time. This might be acceptable for climatologies that are taken  
289 during the same phase of the solar cycle, but there may or may not have been  
290 long-term changes in the MLT region and in the lower atmospheric sources. In  
291 addition, validation would also require comparisons with data obtained using  
292 different measuring techniques.

293 However, a TIDI/UARS comparison is certainly helpful to verify the gen-  
294 eral consistency of both data sets. A similar comparison for the diurnal tides  
295 (Oberheide et al., 2006) yielded an excellent agreement in the spatio-temporal  
296 structure at 95 km although the UARS amplitudes were roughly 50% smaller

297 than those from TIDI. Figure 6 shows the amplitude comparison for the w3  
298 component in January, April, July, and October. TIDI and UARS amplitudes  
299 range from almost zero to 8 m/s with a similar latitudinal distribution in  
300 most cases. The UARS minimum at  $0^\circ$  and the maximum at  $30^\circ\text{N}$  in Jan-  
301 uary are not observed by TIDI but this is not of much concern because the  
302 UARS amplitudes in February (not shown) are very similar to the January  
303 and February amplitudes from TIDI. It may thus be related to the 11-year  
304 time lag between both data sets. TIDI and UARS amplitudes in April have  
305 three maxima that are located within about  $10^\circ$  latitude. The July comparison  
306 shows large amplitudes poleward of  $40^\circ\text{S}$  in both data sets, a second maxi-  
307 mum at low Northern latitudes and another one poleward of  $20^\circ\text{N}$ . Latitudes  
308 of minimum amplitudes differ by  $10^\circ$  only. In October, the UARS maximum  
309 in the Northern Hemisphere is  $20^\circ$  poleward of the TIDI observation but the  
310 UARS and TIDI amplitudes behave nevertheless similar: amplitudes increase  
311 poleward and equatorward of  $40^\circ\text{S}$ , and toward higher Northern latitudes. Be-  
312 cause the UARS error bars are unknown, it is difficult to assess whether the  
313 amplitude difference in the Northern Hemisphere is significant or not.

314 The TIDI/UARS comparison for w1 (Figure 7) is even better. Both data sets  
315 show almost the same latitudinal distribution in January, April, and October.  
316 The comparison in July is less favorable but becomes better in August (not  
317 shown). A more quantitative assessment than discussing pattern similarities is  
318 not meaningful here, owing to the 11-year time lag between the measurements.  
319 Considering that, the amplitude agreement between TIDI and UARS is rather  
320 remarkable. Angelats i Coll and Forbes (2002) established that the nonlinear  
321 interaction between the migrating tide and the Quasi-Stationary Planetary  
322 Wave 1 (QSPW-1) significantly contributes to the generation of the w3 and

323 w1 components observed in the 95 km UARS data. Hence, the same process  
324 will likely be of importance in forcing the tides observed in the TIDI data. The  
325 relative importance of other mechanisms, that is, the latent heat source, and  
326 the height dependence of their imprints upon the tidal fields in the MLT needs  
327 further consideration and requires the comparison with models that account  
328 for these sources.

## 329 **5 Model comparison and tidal forcing**

330 A comparison of the TIDI climatologies to the tidal predictions of the GSWM  
331 and the TIME-GCM allows an interpretation of the observational results in  
332 terms of forcing mechanisms (Table 2), and, in addition, provides a general  
333 assessment of their tidal prediction capabilities. As a climatological, linear  
334 tidal model, GSWM does not account for nonlinear processes such as wave-  
335 wave interaction forcing and it does not produce interannual variations. The  
336 model version used here is described by Hagan and Forbes (2003) and includes  
337 latent heat release in the tropical troposphere due to deep convection as the  
338 only tidal source. GSWM provides monthly amplitudes and phases for 13  
339 diurnal and 13 semidiurnal tidal components (w6 to e6) in the zonal and  
340 meridional wind directions respectively.

341 The latent heat source, on the other hand, is not included in TIME-GCM such  
342 that nonmigrating semidiurnal tides in the model can only come from wave-  
343 wave interactions and/or radiative forcing. Hence, both models account for  
344 different tidal sources and may therefore provide insight into the relative im-  
345 portance of the different forcing mechanisms. As for the nonmigrating diurnal  
346 tides (Hagan and Roble, 2001), it is reasonable to assume that the nonmigrat-

347 ing semidiurnal TIME-GCM response is primarily driven by the interaction  
348 between QSPW-1 and the migrating tide. Zonal asymmetries in ozone and thus  
349 in UV absorption may also contribute but they likely do not play a leading role  
350 in the model. For this study, TIME-GCM was run for the years 2002 and 2003  
351 with the migrating tides at the lower model boundary specified by GSWM  
352 (radiative forcing only) and 10 hPa temperature and geopotential data from  
353 NCEP. The simulations also included realistic solar and geomagnetic forcing  
354 based upon the conditions that prevailed in 2002 and 2003. Daily model out-  
355 put was generated with 1 hour time resolution. Fast Fourier transform then  
356 provides daily tidal amplitudes and phases that were averaged into monthly  
357 bins. Both the GSWM and TIME-GCM data used in the following come from  
358 the same model runs that were used for the diurnal analyses of Oberheide et  
359 al. (2006).

### 360 *5.1 Zonal wind*

361 Figure 8 shows a comparison between the measured and modeled zonal wind  
362 amplitudes as function of month and latitude. The sum of the GSWM and  
363 TIME-GCM amplitudes (without accounting for the relative phasing of both  
364 models) is also provided and may be considered as a proxy for the aggre-  
365 gate effects of latent heat release and wave-wave interaction forced tides, as  
366 predicted by the models. It is quite obvious that the general result is rather  
367 inconclusive. The agreement ranges from good (w3, s0) to moderate (w1, e1,  
368 e2) to poor (w4) thus emphasizing the present achievements and shortcomings  
369 in understanding the nonmigrating semidiurnal tides.

370 For w4, both GSWM and TIME-GCM show symmetric phases about the equa-

371 tor, as observed by TIDI (Figure 2), but they fail to reproduce the observed  
372 double peak structure at 30-40° North and South. TIME-GCM maximizes  
373 at roughly the same time of the year but with amplitudes that are way too  
374 small. GSWM, on the other hand, predicts a low latitude maximum around  
375 boreal summer that is only covertly present in the TIDI data during May. The  
376 model result that latent heat forcing is comparatively more important than  
377 wave-wave interaction is thus not confirmed by the observation.

378 The w3 comparison is much better. GSWM and TIME-GCM together repro-  
379 duce the observed seasonal amplitude variation with maxima around equinoxes  
380 and boreal winter. However, neither model predicts the boreal summer peaks  
381 in TIDI and they underestimate the observed amplitudes by about a factor  
382 of two. Apart from these differences and the general model tendency to peak  
383 more poleward, the observation is consistent with the model result that both  
384 latent heat release and wave-wave interaction are about equally important in  
385 forcing the w3 zonal component over the course of the year. TIME-GCM re-  
386 sponse is likely caused by migrating tide (w2) - QSPW-1 interaction that can  
387 produce w1 and w3 as secondary waves.

388 For w1, both models reproduce the seasonal amplitude variation at higher  
389 latitudes reasonably well with roughly the same contributions. As for w3,  
390 GSWM and TIME-GCM show a tendency to peak more poleward compared  
391 to TIDI. Observed and modeled amplitudes have about the same magnitude.  
392 The major difference is the absence of the observed low-latitude maxima. Such  
393 a maximum is weakly present in TIME-GCM (105 km, September, not shown)  
394 but in any case much too small compared to TIDI.

395 The s0 comparison is better, but again, both models maximize at latitudes

396 more poleward than in the observation. In this case, GSWM accounts for  
397 about two third of the total model amplitudes. Hence, latent heat release in  
398 the tropical troposphere is the comparatively more important tidal source.  
399 TIME-GCM response may either come from w2 - QSPW-2 interaction and/or  
400 w1 - QSPW-1 interaction. A recently submitted paper by Liu et al. (2007)  
401 suggests that interactions between nonmigrating tides and QSPWs may lead to  
402 substantial secondary wave generation in TIME-GCM, at least for the diurnal  
403 tides. Magnitude and seasonal variation of the combined GSWM and TIME-  
404 GCM amplitudes agree quite well with the TIDI result.

405 The modeled e1 amplitudes from GSWM and TIME-GCM are quite different:  
406 the former predicts two peaks at 50° latitude and the latter one a smaller  
407 maximum around the equator. Similar patterns can be found in the TIDI  
408 data, although the temporal evolution of the observed small equatorial ampli-  
409 tudes is different. However, the combined model amplitudes agree well with  
410 TIDI in the Southern Hemisphere. In contrast to that, the observed temporal  
411 evolution in the Northern Hemisphere (boreal summer maximum) is different  
412 to the modeled one (boreal summer minimum). Nevertheless, the comparison  
413 indicates that the e1 response at higher latitudes is governed by latent heat  
414 release and the equatorial response by wave-wave interaction. As for s0, the  
415 latter would require secondary wave interaction between nonmigrating tides  
416 and QSPWs.

417 For e2, TIME-GCM response is small such that this component is largely  
418 driven by latent heat release alone. The predicted (GSWM) maximum in fall  
419 occurs simultaneously to the observed one with the winter/spring maximum in  
420 TIDI occurring somewhat earlier than in the model. GSWM underestimates  
421 the e2 amplitude by roughly a factor of two. The model, although peaking

422 slightly more poleward than the observation, reproduces the boreal winter  
423 peak latitudes quite well. However, the observed maxima in fall are located at  
424 lower latitudes compared to the model prediction.

## 425 *5.2 Meridional wind*

426 Much of what has been said for the zonal wind also holds for the meridional  
427 wind (Figure 9), in particular for the relative importance of both latent heat  
428 and wave-wave interaction forcing. The model results for the meridional wind  
429 show the same tendency to maximize at slightly higher latitudes as compared  
430 to the observation. W4 is again poorly represented by the models. The w3  
431 model predictions underestimate the observation by a factor of two but their  
432 combined amplitudes capture the equatorial maximum quite well. As before,  
433 the TIDI boreal summer peak is missing. For w1, the models do better in  
434 reproducing the latitudinal structure as compared to the zonal wind: the ob-  
435 served 4 peak structure is quite evident during most parts of the year. The  
436 model predictions for s0 lack the observed fall equinox maxima but basically  
437 capture the occurrence of low latitude maxima although the latter are more  
438 pronounced in TIDI. The combined models predict about the right latitudinal  
439 distribution for e1, but with a similar shortcoming as in the zonal wind: the  
440 observed boreal summer maximum is not present in the models. TIME-GCM  
441 for e2 is negligible with GSWM underestimating the amplitude by a factor of  
442 two, as in the zonal wind. The boreal summer maximum has no complement  
443 in the model. In addition, TIDI has the largest amplitudes at the equator  
444 whereas the model amplitudes at 40° are larger than those at the equator.

445 One possible reason for the model/observation discrepancies and the partly

446 inconclusive results might be that the approach does not account for the effects  
447 of latent heat forced nonmigrating tide - QSPW interaction. However, tidal  
448 forcing and dissipation schemes may also play an important role. With the  
449 abovementioned constraints, Table 2 summarizes the likely forcing of the six  
450 nonmigrating semidiurnal components derived from the TIDI data.

## 451 **6 Summary and conclusions**

452 The TIDI wind data allow for the first time a detailed analysis of the morphol-  
453 ogy of nonmigrating semidiurnal tides over a range of MLT altitudes. Monthly  
454 climatologies for 6 components in the zonal and meridional wind directions  
455 have been derived between 85 and 105 km altitude. The present analysis covers  
456 the latitude range between 45°S and 45°N and will likely be extended to higher  
457 latitudes (60°) in the future, although planetary wave aliasing may become an  
458 issue there. At 95 km, the TIDI results agree remarkably well with 1991-1994  
459 results from UARS. During boreal winter, amplitudes of a single component  
460 can easily reach 10 m/s such that the aggregate effects of all nonmigrating  
461 tides may reach or even exceed the magnitude of the migrating tide although  
462 the latter could not be analyzed.

463 A comparative analysis with the tidal predictions of two models of differing  
464 characters, the GSWM and the TIME-GCM, indicates that wave-wave inter-  
465 action forcing and latent heat release in the tropical troposphere are about  
466 equally important in forcing the w3, w1, and s0 components. The eastward  
467 propagating components are primarily forced by latent heat release, similar  
468 to the findings for the diurnal components (Oberheide et al., 2006). There  
469 are, however, several shortcomings in our present model understanding of the

470 semidiurnal nonmigrating tides that lead to model/observation discrepancies  
471 that are generally larger than those for the diurnal tides. Reasons for that need  
472 to be studied in more detail in the future, but both the interaction between  
473 latent heat release forced tides and QSPWs and the model parameterization  
474 schemes likely play a role. Results from the ongoing Climate and Weather of  
475 the Sun-Earth System (CAWSES) global observing campaign on tides together  
476 with the TIDI climatologies and similar analyses of SABER temperatures are  
477 expected to give some guidance for future model improvements.

478 It is nevertheless quite clear that nonmigrating tides provide an effective mech-  
479 anism to transport the signal of large scale weather systems from the tropo-  
480 sphere into the MLT region where they play a decisive role in driving the MLT  
481 dynamics. E-region dynamo electric field modulation may then further trans-  
482 port the tidal signal into the F-region. Observational and modeling efforts to  
483 understand this vertical coupling over an altitude range of 400 km are still in  
484 an early stage but the tidal climatologies from TIDI and SABER will certainly  
485 help to get a better hold on the underlying physics in the future.

## 486 **Acknowledgments**

487 We wish to thank H.-L. Liu for comments on an initial draft of this manuscript.  
488 J. Oberheide's work is supported by the DFG priority program CAWSES  
489 through grant OB 299/2-1. The National Center for Atmospheric Research is  
490 sponsored by the NSF.

491 **References**

- 492 Angelats i Coll, M., Forbes, J.M., 2002. Nonlinear interactions in the upper  
493 atmosphere: The  $s=1$  and  $s=3$  nonmigrating semidiurnal tides. *Journal of*  
494 *Geophysical Research* 107 (A8), 1157, doi:10.1029/2001JA900179.
- 495 Baumgaertner, A.J.G., Jarvis, M.J., McDonald, A.J., Fraser, G.J., 2006. Ob-  
496 servations of the wavenumber 1 and 2 components of the semi-diurnal tide  
497 over Antarctica. *Journal of Atmospheric and Solar-Terrestrial Physics*, 68  
498 (11), 1195-1214, doi:10.1016/j.jastp.2006.03.001.
- 499 Chapman, S., Lindzen, R.S., 1970. *Atmospheric Tides*. D. Reidel, Norwell,  
500 Mass.
- 501 Cierpik, K.M., Forbes, J.M., Miyahara, S., Miyoshi, Y., Fahrutdinova, A., Ja-  
502 cobi, C., Manson, A., Meek, C., Mitchell, N.J., Portnyagin, Y., 2003. Lon-  
503 gitude variability of the solar semidiurnal tide in the lower thermosphere  
504 through assimilation of ground- and space-based wind measurements. *Jour-*  
505 *nal of Geophysical Research* 108 (A5), 1202, doi:10.1029/2002JA009349.
- 506 Forbes, J.M., Wu, D., 2006. Solar Tides as Revealed by Measurements of  
507 Mesosphere Temperature by the MLS Experiment on UARS. *Journal of the*  
508 *Atmospheric Sciences* 63 (7), 1776-1797, doi:10.1175/JAS3724.1.
- 509 Forbes, J.M., Portnyagin, Yu.I., Makarov, N.A., Palo, S.E., Merzlyakov, E.G.,  
510 Zhang, X., 1999. Dynamics of the lower thermosphere over South Pole from  
511 meteor radar wind measurements. *Earth, Planets and Space* 51 (7-8), 611-  
512 620.
- 513 Forbes, J.M., Zhang, X., Ward, W.E., Talaat, E.R., 2003. Nonmigrating diur-  
514 nal tides in the thermosphere. *Journal of Geophysical Research* 108 (A1),  
515 1033, doi:10.1029/2002JA009262.
- 516 Forbes, J.M., Russell, J., Miyahara, S., Zhang, X., Palo, S., Mlynczak, M.,

- 517 Mertens, C.J., Hagan, M.E., 2006. Troposphere-thermosphere tidal cou-  
518 pling as measured by the SABER instrument on TIMED during July-  
519 September 2002. *Journal of Geophysical Research* 111 (A10), A10S06,  
520 doi:10.1029/2005JA0011492.
- 521 Grieger, N., Volodin, E.M., Schmitz, G., Hofmann, P., Manson, A.H.,  
522 Fritts, D.C., Igarashi, K., Singer, W., 2002. General circulation model re-  
523 sults on migrating and nonmigrating tides in the mesosphere and lower  
524 thermosphere. Part I: comparison with observations. *Journal of Atmo-  
525 spheric and Solar-Terrestrial Physics* 64 (8-11), 897-911, doi:10.1016/S1364-  
526 6826(02)00045-7
- 527 Hagan, M.E., Forbes, J.M., 2002. Migrating and nonmigrating diurnal  
528 tides in the middle and upper atmosphere excited by tropospheric la-  
529 tent heat release. *Journal of Geophysical Research*, 107 (D24), 4754,  
530 doi:10.1029/2001JD001236.
- 531 Hagan, M.E., Forbes, J.M., 2003. Migrating and nonmigrating semid-  
532 urnal tides in the upper atmosphere excited by tropospheric la-  
533 tent heat release. *Journal of Geophysical Research* 108 (A2), 1062,  
534 doi:10.1029/2002JA009466.
- 535 Hagan, M.E., Roble, R.G., 2001. Modeling the diurnal tidal variability with  
536 the National Center for Atmospheric Research thermosphere-ionosphere-  
537 mesosphere-electrodynamics general circulation model. *Journal of Geophys-  
538 ical Research*, 106, 24,869-24,882.
- 539 Hibbins, R.E., Espy, P.J., Jarvis, M.J., 2006. Mean winds and tides in  
540 the mesosphere and lower thermosphere above Halley, Antarctica. *Jour-  
541 nal of Atmospheric and Solar-Terrestrial Physics* 68 (3-5), 436-444,  
542 doi:10.1016/j.jastp.2005.02.030.
- 543 Huang, F.T., Reber, C.A., 2004. Nonmigrating semidiurnal and diurnal

544 tides at 95 km based on wind measurements from the High Resolution  
545 Doppler Imager on UARS. *Journal of Geophysical Research* 109 (D10110),  
546 doi:10.1029/2003JD004442.

547 Immel, T.J., Sagawa, E., England, S.L., Henderson, S.B., Hagan, M.E., Mende,  
548 S.B., Frey, H.U., Swenson, C.M., Paxton, L.J., 2006. Control of ionospheric  
549 morphology by atmospheric tides. *Geophysical Research Letters*, 33 (15),  
550 L15108, doi:10.1029/2006GL026161.

551 Killeen, T.L., Wu, Q., Solomon, S.C., Ortland, D.A., Skinner, W.R.,  
552 Niciejewski, R.J., Gell, D.A., 2006. TIMED Doppler Interferometer:  
553 Overview and recent results. *Journal of Geophysical Research* 111, A10S01,  
554 doi:10.1029/2005JA011484.

555 Lau, E., Avery, S.K., Avery, J.P., Palo, S.E., Makarov, N.A., 2006. Tidal  
556 analysis of meridional winds at the South Pole using a VHF interfer-  
557 ometric meteor radar. *Journal of Geophysical Research* 111, D16108,  
558 doi:10.1029/2005JD006734.

559 Lieberman, R.S., Oberheide, J., Hagan, M.E., Remsberg, E.E., Gordley, L.L.,  
560 2004. Variability of diurnal tides and planetary waves during November  
561 1978 - May 1979. *Journal of Atmospheric and Solar-Terrestrial Physics*, 66,  
562 517-528.

563 Liu, H.-L., Li, T., She, C.-Y., Oberheide, J., Wu, Q., Hagan, M.E., Xu, J.,  
564 Roble, R.G., Mlynczak, M.G., Russell III, J.M., 2007. Comparative Study of  
565 Short Term Tidal Variability. *Journal of Geophysical Research*, submitted.

566 Manson, A.H., Meek, C., Hagan, M., Zhang, X., Luo, Y., 2004. Global distri-  
567 butions of diurnal and semidiurnal tides: Observations from HRDI-UARS of  
568 the MLT region and comparison with GSWM-02 (migrating, nonmigrating  
569 components). *Annales Geophysicae* 22 (5), 1529-1548.

570 Mayr, H.G., Mengel, J.G., Talaat, E.R., Porter, H.S., Chan, K.L., 2005. Meso-

571 spheric non-migrating tides generated with planetary waves: I. Characteris-  
572 tics. *Journal of Atmospheric and Solar-Terrestrial Physics* 67 (11), 959-980,  
573 doi:10.1016/j.jastp.2005.03.002.

574 Murphy, D.J., Tsutsumi, M., Riggin, D.M., Jones, G.O.L., Vincent, R.A.,  
575 Hagan, M.E., Avery, S.K., 2003. Observations of a nonmigrating component  
576 of the semidiurnal tide over Antarctica. *Journal of Geophysical Research* 108  
577 (D8), 4241, doi:10.1029/2002JD003077.

578 Oberheide, J., Hagan, M.E., Roble, R.G., Offermann, D., 2002. The sources  
579 of nonmigrating tides in the tropical middle atmosphere. *Journal of Geo-*  
580 *physical Research*, 107 (D21), 4567, doi:10.1029/2002JD002220.

581 Oberheide, J., Hagan, M.E., Roble, R.G., 2003. Tidal signatures and aliasing  
582 in temperature data from slowly precessing satellites. *Journal of Geophysical*  
583 *Research* 108 (A2), 1055, doi:10.1029/2002JA009585.

584 Oberheide, J., Wu, Q., Killeen, T.L, Hagan, M.E., Roble, R.G., 2006. Di-  
585 urnal nonmigrating tides from TIMED Doppler Interferometer wind data:  
586 Monthly climatologies and seasonal variations. *Journal of Geophysical Re-*  
587 *search* 111, A10S03, doi:10.1029/2005JA011491.

588 Pancheva, D., and 27 co-authors, 2002. Global-scale tidal structure in the  
589 mesosphere and lower thermosphere during the PSMOS campaign of June-  
590 August 1999 and comparisons with the global-scale wave model. *Jour-*  
591 *nal of Atmospheric and Solar-Terrestrial Physics* 64 (8-11), 1011-1035,  
592 doi:10.1016/S1364-6826(02)00054-8.

593 Roble, R.G., Ridley, E.C., 1994. A thermosphere-ionosphere-mesosphere-  
594 electrodynamics general circulation model (TIME-GCM): Equinox solar cy-  
595 cle minimum simulations (30-500 km). *Geophysical Research Letters*, 21,  
596 417-420, doi:10.1029/93GL03391.

597 Ward, W.E., 1999. A simple model of diurnal variations in the mesospheric

598 oxygen nightglow. *Geophysical Research Letters*, 26, 3565-3568.

599 Ward, W.E., Fomichev, V.I., Beagley, S., 2005. Nonmigrating tides in  
600 equinox temperature fields from the Extended Canadian Middle At-  
601 mosphere Model (CMAM). *Geophysical Research Letters* 32, L03803,  
602 doi:10.1029/2004GL021466.

603 Wu, Q., Killeen, T.L., Nozawa, S., McEwen, D., Guo, W., Solomon, S.C., 2003.  
604 Observations of mesospheric neutral wind 12-hour wave in the Northern  
605 Polar Cap. *Journal of Atmospheric and Solar-Terrestrial Physics* 65 (8),  
606 971-978, doi:10.1016/S1364-6826(03)00116-0.

607 Wu, Q., Killeen, T.L., Ortland, D.A., Solomon, S.C., Gablehouse, R.D., John-  
608 son, R.M., Skinner, W.R., Niciejewski, R.J., Franke, S.J., 2006. TIMED  
609 Doppler Interferometer (TIDI) observations of migrating diurnal and semi-  
610 diurnal tides. *Journal of Atmospheric and Solar-Terrestrial Physics*, 68 (3-5),  
611 408-417, doi:10.1016/j.jastp.2005.02.031.

612 Yamashita, K., Miyahara, S., Miyoshi, Y., Kawano, K., Ninomiya, J., 2002.  
613 Seasonal variation of non-migrating semidiurnal tide in the polar MLT  
614 region in a general circulation model. *Journal of Atmospheric and Solar-  
615 Terrestrial Physics* 64 (8-11), 1083-1094, doi:10.1016/S1364-6826(02)00059-  
616 7.

617 Zhang, X.L., Forbes, J.M., Hagan, M.E., Russell, J.M., Palo, S.E., Mertens,  
618 C.J., Mlynczak, M.G., 2006. Monthly tidal temperatures 20-120 km  
619 from TIMED/SABER. *Journal of Geophysical Research* 111, A10S08,  
620 doi:10.1029/2005JA011504.

Table 1

Semidiurnal amplitude and phase errors for the meridional ( $v$ ) and zonal ( $u$ ) wind.

For scaling factors see text.

component	scaling factor		amplitude accuracy		amplitude precision		phase precision	
	$v$	$u$	$v$ [%]	$u$ [%]	$v$ [ $\frac{m}{s}$ ]	$u$ [ $\frac{m}{s}$ ]	$v$ [hours]	$u$ [hours]
w4	1.50	1.54	17	14	0.8	0.7	1.8	1.6
w3	1.27	1.25	19	17	0.8	0.7	2.0	2.0
w1	1.29	1.33	17	23	0.9	0.7	2.0	1.9
s0	1.51	1.54	13	18	0.8	0.6	2.0	2.0
e1	2.05	2.10	20	13	0.7	0.5	2.2	2.0
e2	3.22	3.10	13	17	0.8	0.6	2.3	1.7

Table 2

Tidal forcing as derived from the observation/model comparison.

---

component	forcing
w4	inconclusive; poor model agreement
w3	latent heat and wave-wave interaction about equally important
w1	”
s0	”
e1	latent heat more important
e2	latent heat alone

---

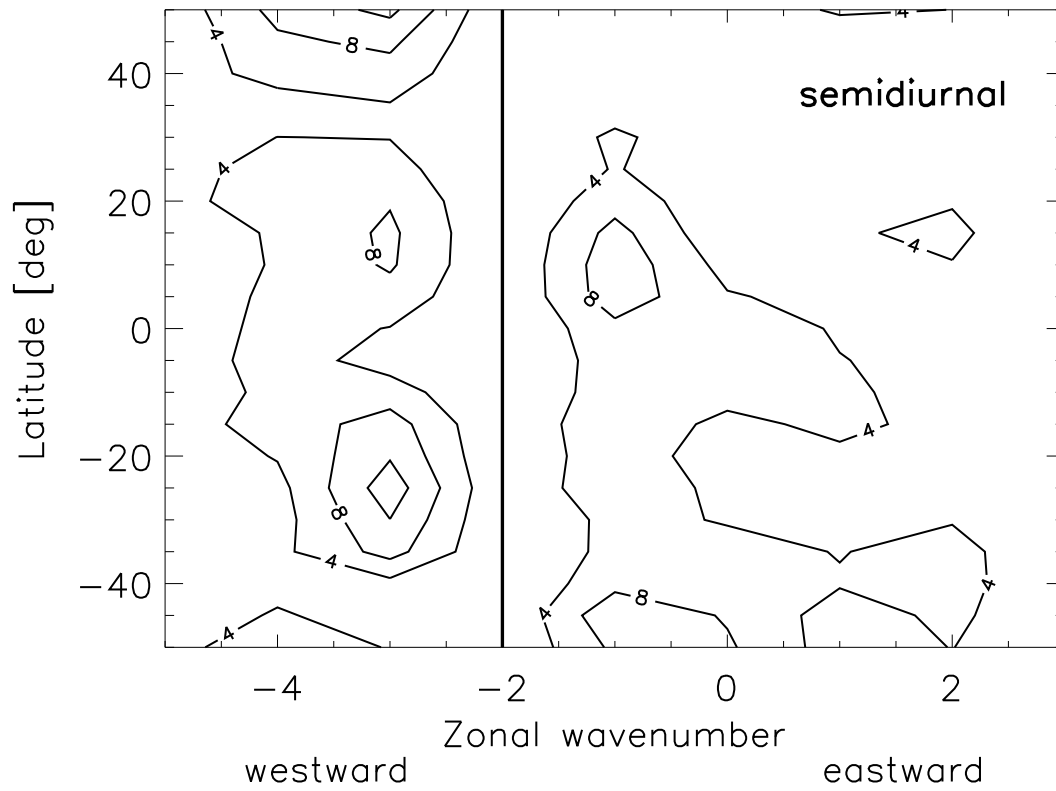


Fig. 1. Amplitudes from TIDI composite data for the period 15 January 2004 to 18 March 2004 (later assigned to 15 February 2004) at 95 km for the meridional wind. The position of the migrating component (that has not been analyzed) is indicated by the thick vertical line.

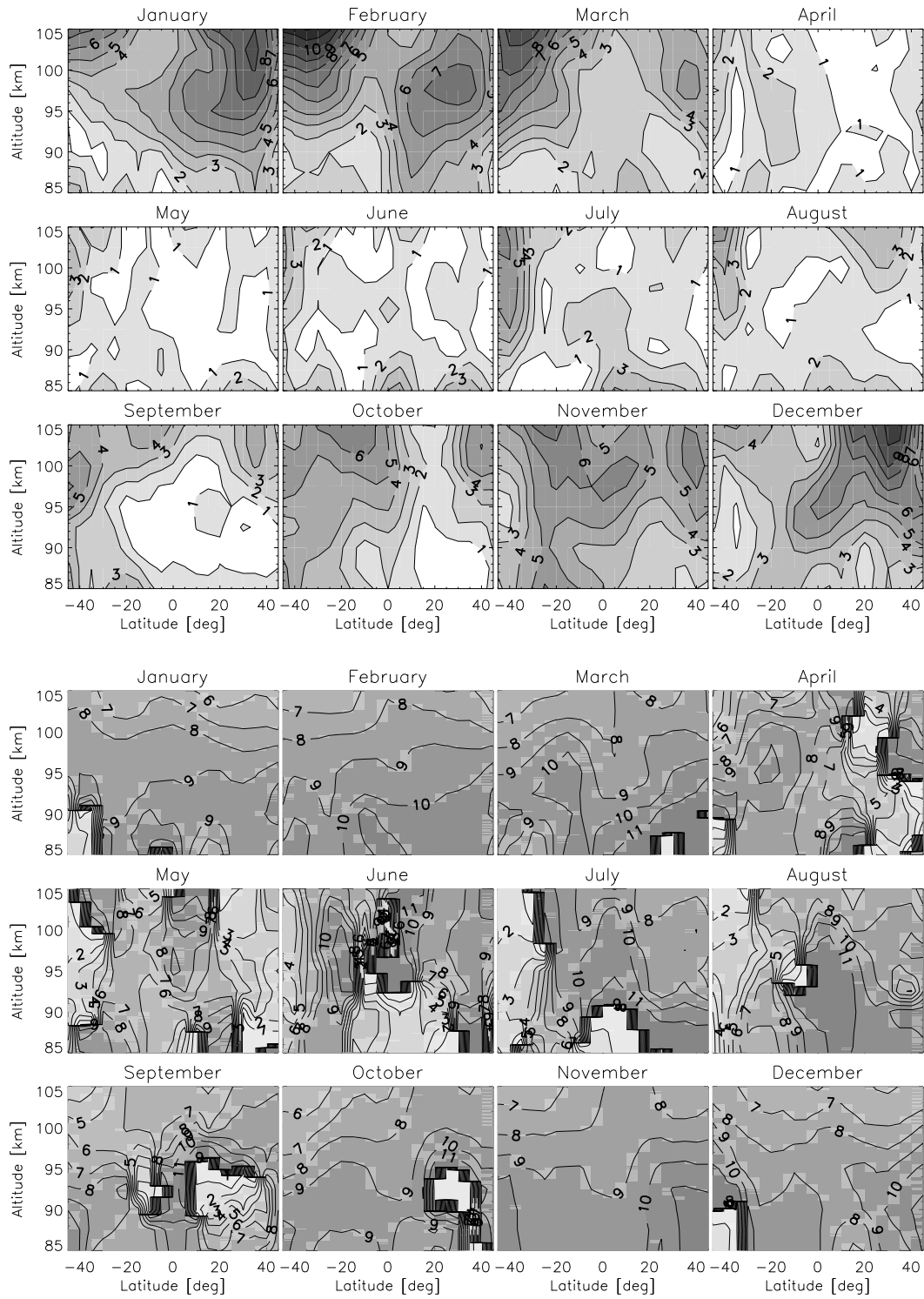


Fig. 2. Monthly mean semidiurnal amplitudes (m/s, top) and phases (Universal time of maximum at  $0^\circ$  longitude in hours, bottom) for the w4 zonal wind component. Multiple phase contours adjacent to each other indicate the transition from 0 to 12 hours. Contour intervals are 1 m/s and 1 hour respectively.

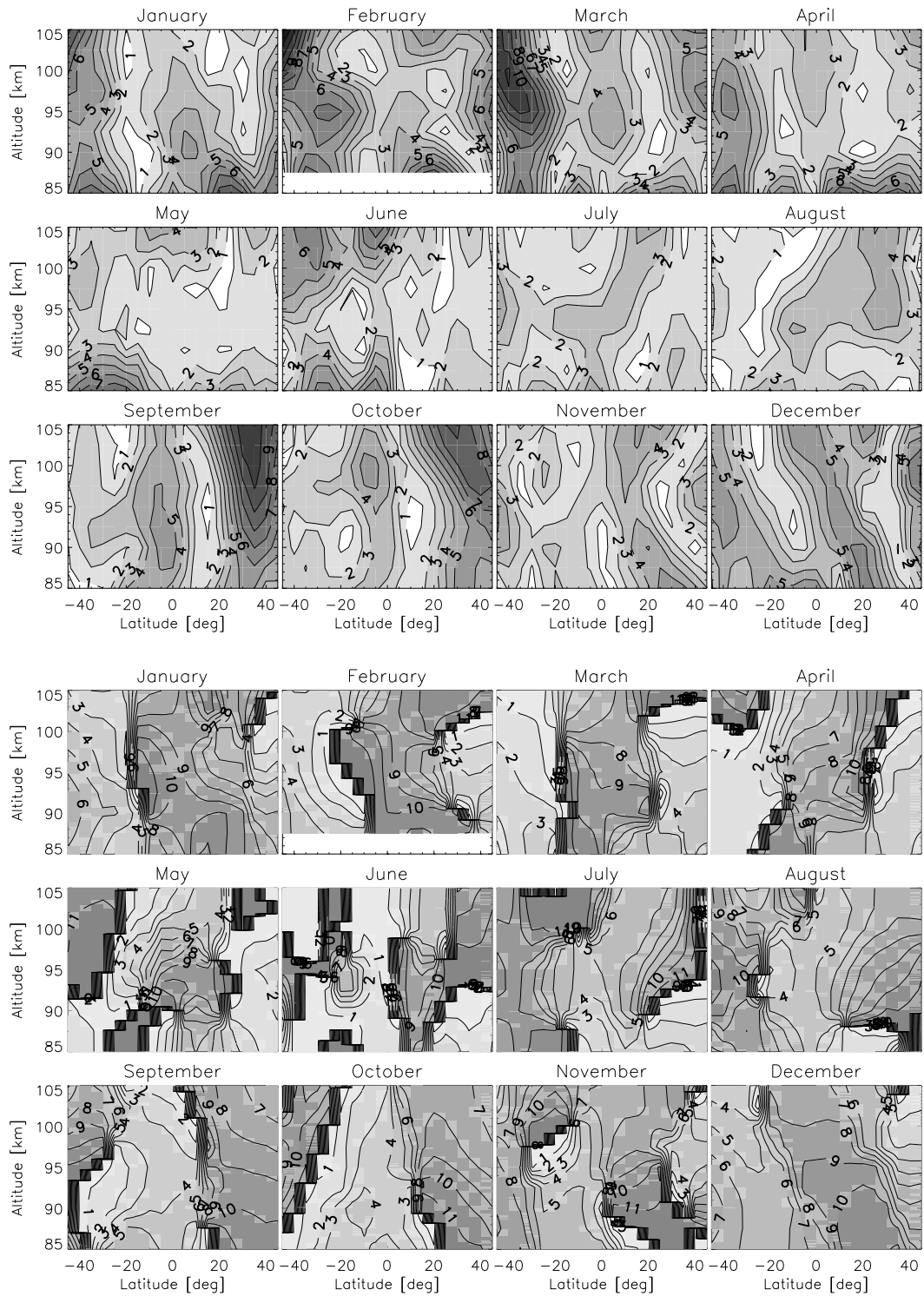


Fig. 3. As Fig. 2, but for the w3 meridional wind component.

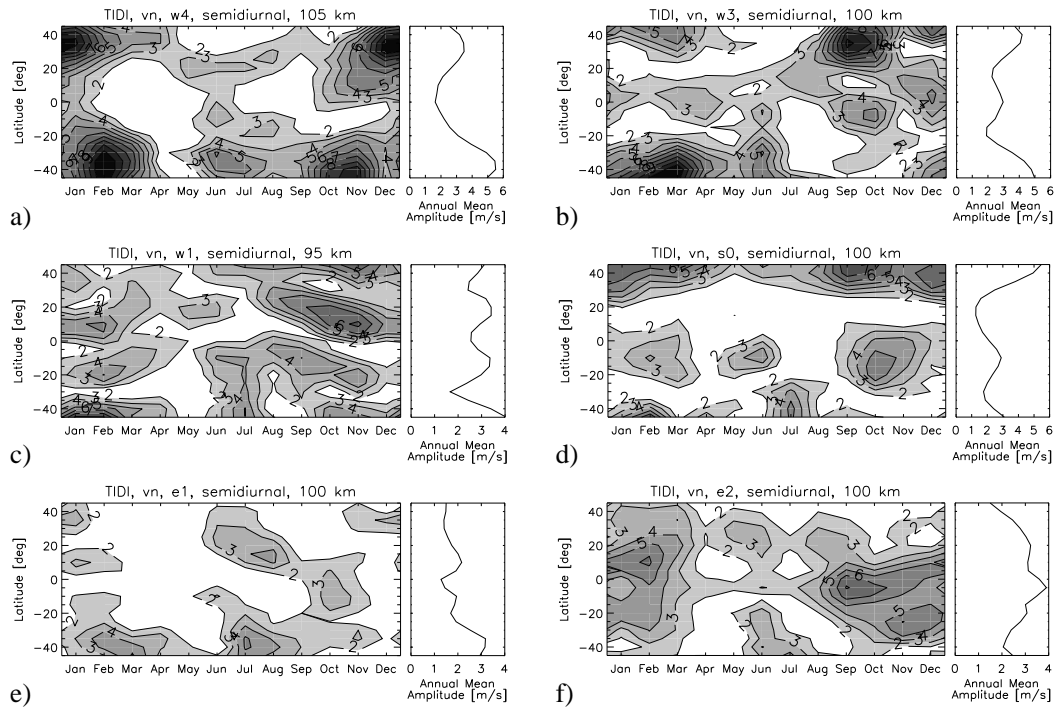


Fig. 4. Time evolution of semidiurnal amplitudes for the meridional wind and annual mean amplitudes. Contour interval is 1 m/s. Components are given at different altitudes. a) w4, 105 km; b) w3, 100 km; c) w1, 95 km; d) s0, 100 km; e) e1, 100 km; f) e2, 100 km.

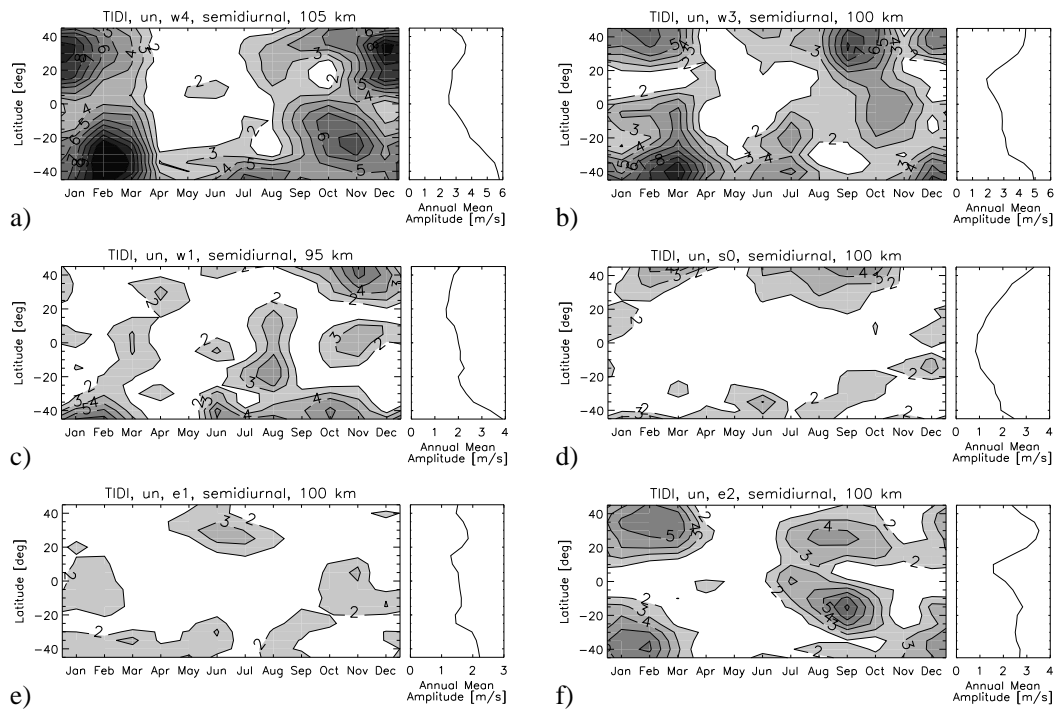


Fig. 5. As Fig. 4, but for the zonal wind.

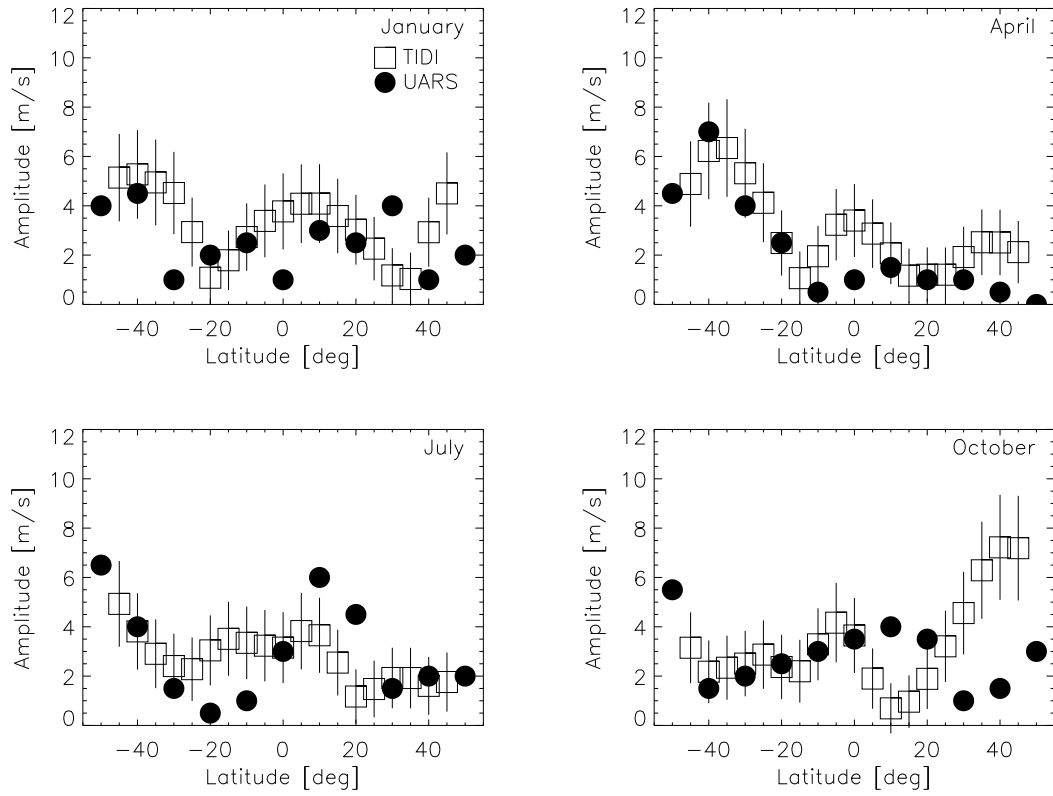


Fig. 6. W3 meridional wind amplitudes from TIDI and UARS (Angelats i Coll and Forbes, 2002) at 95 km for equinox and solstice conditions. TIDI error bars are from Tab. 1. UARS error bars are unknown.

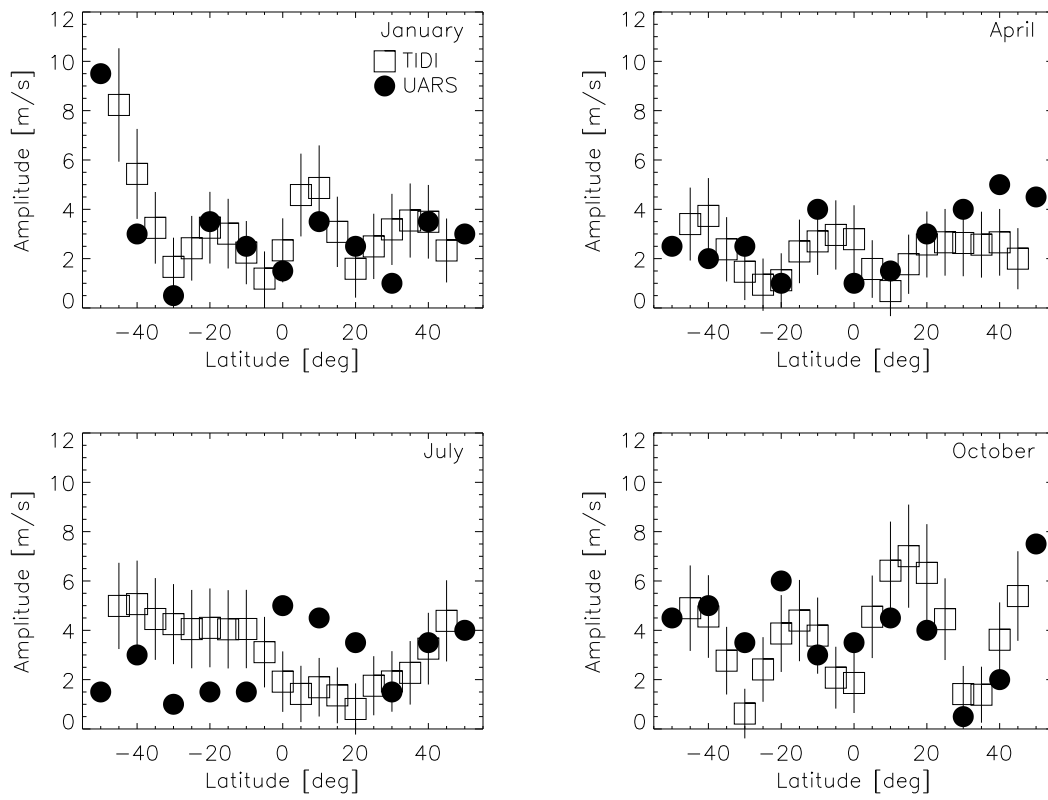


Fig. 7. As Fig. 6, but for the w1 meridional component.

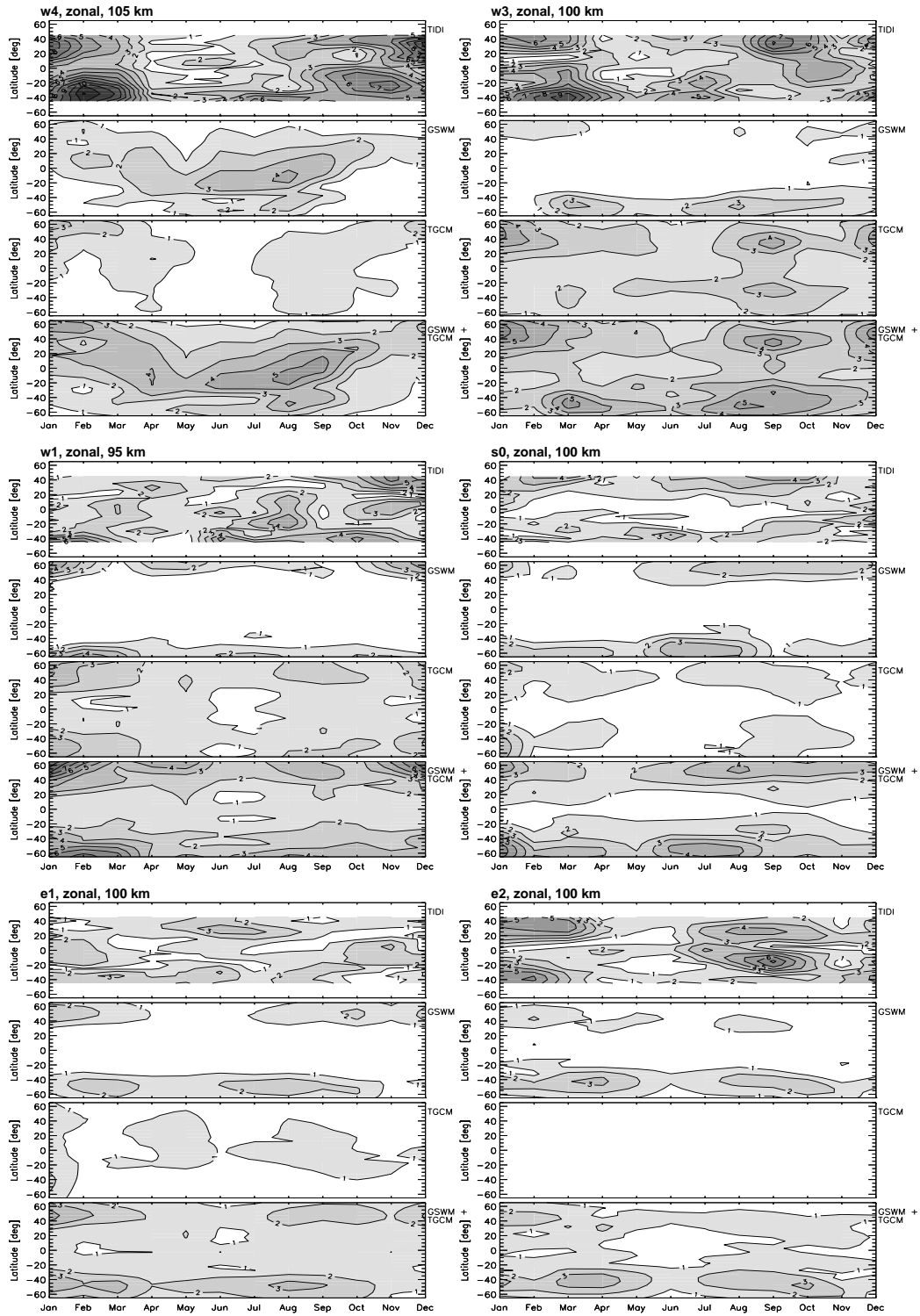


Fig. 8. Amplitudes of the w4, w3, w1, s0, e1, e2 zonal wind components from TIDI, GSWM, TIME-GCM, sum of GSWM and TIME-GCM. Contour interval is 1 m/s.

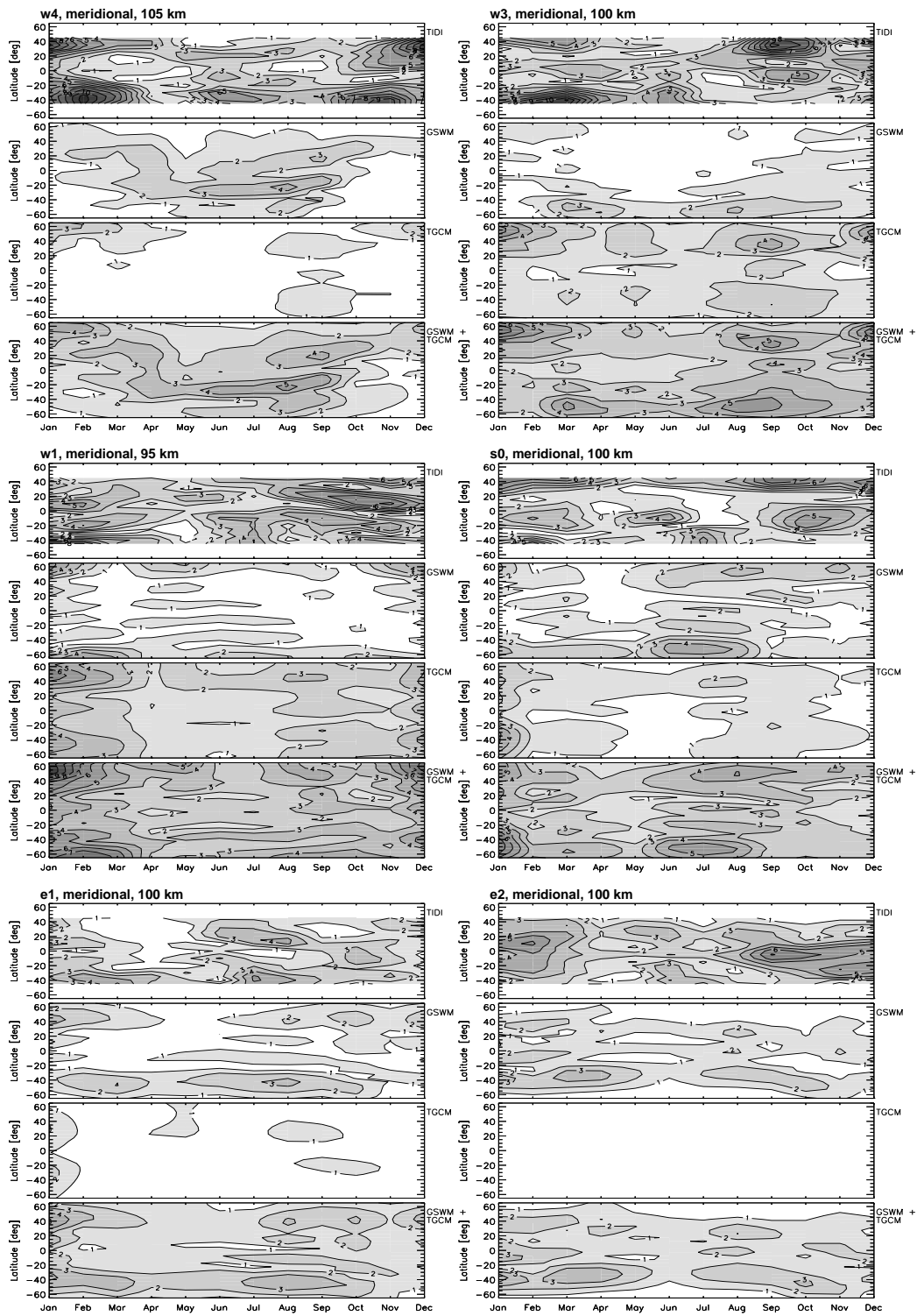


Fig. 9. As Fig. 8, but for the meridional wind components.